Link between geometrical and physical property changes along Nankai Trough with slow earthquake activity revealed by dense reflection survey

Paul Caesar M. Flores[1,2], Shuichi Kodaira[2,1], Gaku Kimura[2], Kazuya Shiraishi[2], Yasuyuki Nakamura[2], Gou Fujie[2], Tetsuo No[2], and Yuka Kaiho[2]

[1]Graduate School of Environment and Information Sciences, Yokohama National University, Yokohama, Japan.

[2]Research Institute for Marine Geodynamics, Japan Agency for Marine-Earth Science and Technology, Yokohama, Japan.

Corresponding author: Paul Caesar M. Flores (paul-flores-bj@ynu.jp)

Key Points:

- A smooth decollement due to absence of subducted seamounts or bathymetric highs, and low pore fluid pressure results in a slow earthquake gap.
- Slow earthquakes don't always occur in areas of high pore pressure but in combination with other variables like decollement roughness.
- The low taper angle off Muroto indicates a wide zone of low friction and high pore pressure possibly associated with subducted seamounts.

Abstract

We examined the possible factors affecting the spatial distribution of very low frequency earthquakes and tremors in the shallow megathrust of Nankai Trough (<30 km) using a dense network of prestack depth migrated profiles at the frontal wedge. Geometrical parameters examined were decollement roughness, taper angle, and underthrust thickness. Physical properties such as effective basal friction (μ_b) and pore pressure ratio (λ^*) were calculated from the taper angle and p-wave velocity. Regions of low λ^* (0.39±0.08) and smooth decollement showed no slow earthquake activity. In contrast, high activity of slow earthquakes was observed in areas with a rough decollement due to the presence of subducted seamounts or bathymetric highs. The low taper angle (3.8°) off Muroto where slow earthquakes also occur translates to a wide zone of low μ_b (0.21±0.06) and high λ^* (0.66±0.06). However, our results also show that slow earthquakes don't always occur in areas with high λ^*.

Plain Language Summary

Slow earthquakes such as very low frequency earthquakes and tremors are different than typical earthquakes because they occur longer and can last for more than several days. They have been reported in numerous subduction zones around the world and the study of slow earthquakes has recently gained attention because they have been suggested as precursors to larger earthquakes albeit on rare occasions. Slow earthquakes show a clustered distribution in the Nankai Trough. We used a dense network of seismic reflection data acquired at the shallow portion of the Nankai Trough to examine why some areas have high activity and some areas have no activity. Our results showed that areas with no slow earthquake activity have a smooth decollement and low pore fluid pressure. On the other hand, areas with high slow earthquake activity have a rough decollement. The occurrence of slow earthquakes has been typically associated with high pore fluid pressure because it allows the two slabs of rock to slide easier. However, our results suggest that high pore fluid pressure may not always be a prerequisite for slow earthquakes to occur.

1 Introduction

Slow earthquakes were discovered approximately 20 years ago, and they differ from the typical earthquakes because of their longer duration than regular earthquakes with the same seismic moment (Ide et al., 2007; Ide and Beroza, 2023). They're broadly categorized into two categories, namely, seismic slow earthquakes and geodetic slow earthquakes because these phenomena can be observed by seismometers and geodetic instruments, respectively (Obara, 2020). Very low frequency earthquakes (VLFE) and tremors, which are types of seismic slow earthquakes, have been detected in the shallow megathrust of the Nankai Trough (<30 km) and show a clustered distribution (Figure 1) (Nakano et al. 2018; Takemura et al. 2019a,b; Takemura et al. 2022a,b; Ogiso and Tamaribuchi 2022; Tamaribuchi et al. 2022). Previous studies have suggested possible factors affecting the spatial distribution of VLFEs and tremors such as the presence of a subducted seamount (Takemura et al., 2019a; Sun et al., 2020; Baba et al., 2023), pore fluid pressure (Kodaira et al., 2004; Kitajima and Saffer, 2012; Hirose et al., 2021), sediment thickness and lithology (Ike et al., 2008; Tilley et al., 2021; Park and Jamali-Hondori, 2023) and slip-deficit rate (Yokota et al., 2016).

Numerous mechanisms have been proposed to explain the relationship between seamount subduction and slow earthquake activity. Wang and Bilek (2011) proposed that the rough topography associated with the presence of a seamount creates a fracture network which promotes the occurrence of aseismic creep. Numerical modeling by Ellis et al. (2015) proposed that fluid overpressure develops on the landward side of the seamount, which promotes slow earthquake activity. On the other hand, numerical modeling by Sun et al. (2020) showed that a stress shadow develops on the seaward side of the seamount which leads to anomalously high sediment porosity and thereby promoting slow earthquake activity. In the Hikurangi margin in New Zealand, Chesley et al. (2021) utilized electrical resistivity to propose that slow earthquakes are generated by fluid migration from the subducted seamount. Nakamura et al. (2022) reported the presence of several seamounts on top of a subducted large ridge system off Muroto (Figure 1). This brings into question the effect of multiple subducted seamounts with slow earthquake activity which is not commonly discussed in previous studies.

Pore fluid pressure is an important control on the strength and sliding stability of the decollement (Davis et al., 1983; Dahlen et al., 1984). Elevated pore fluid pressure has been commonly used to explain the occurrence of slow earthquakes (Liu and Rice, 2007; Kitajima and Saffer, 2012; Hirose et al. 2021) because it influences the critical stiffness of a fault such that it becomes closer to elastic stiffness of the surrounding rock for a given temperature and pressure condition, which is a mechanical perquisite for slow earthquake generation (Leeman et al., 2016; Okamoto et al., 2020). High pore pressures off Muroto where slow earthquakes occur have already been predicted by previous studies from p-wave velocity (Tsuji et al., 2008; Tobin and Saffer, 2009) and low taper angle (Kimura et al., 2007; Park et al., 2014), and recently been confirmed by Hirose et al. (2021) through drilling. The elevated pore pressure is suggested to be caused by the lithology of the underthrust sediments (Saffer, 2010). However, it is important to note that there is a lack of comprehensive understanding on the nature of pore fluid pressures associated with slow earthquake generation (Park and Jamali-Hondori, 2023). Previous studies that used seismic velocity to estimate pore pressure only used one transect, and borehole data is also site-specific and may not be representative for an entire region.

Slow earthquakes have been studied extensively and they have been linked to possibly trigger megathrust earthquakes (Kato et al., 2012) or accommodate plate motion (Araki et al., 2017). However, the physical mechanism for slow earthquake generation remains unclear (Nishikawa et al., 2023). The Nankai Trough has been the subject of numerous geological and geophysical research for several decades. The dense reflection survey (~4-8 km spacing) acquired from 2018 to 2020 (Figure 1) provides a 3D view of the subsurface and it provides an excellent laboratory to study the possible factors affecting the slow earthquake activity. In this study, we examined the geometrical changes (i.e. decollement roughness, taper angle, and underthrust thickness) and physical property changes (i.e. effective friction and pore fluid pressure) along Nankai Trough to explain the spatial distribution of slow earthquakes in the shallow megathrust (<30 km) and propose a possible mechanism for slow earthquake generation.

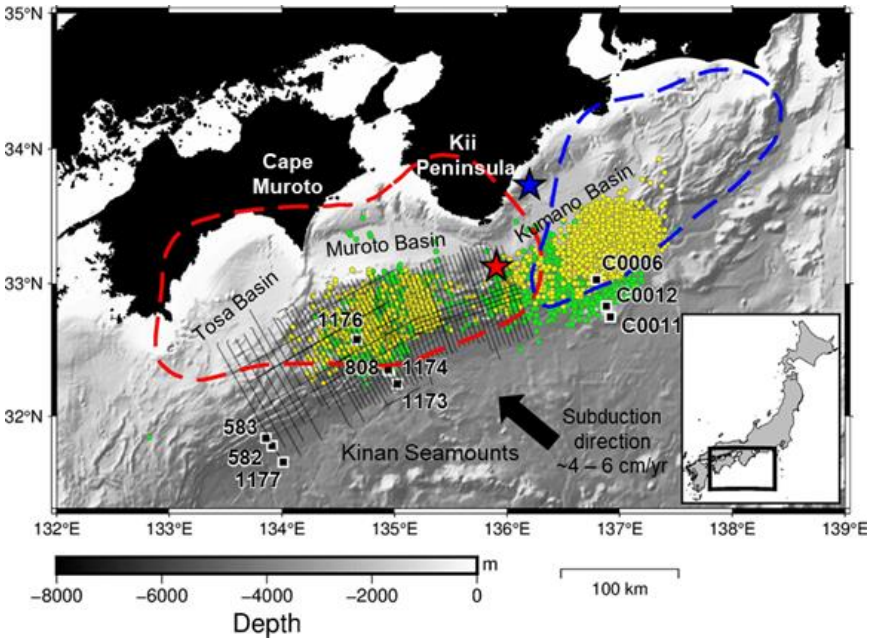

104

105 **Figure 1. (a) Survey lines, from west to east, of the KM20-05, KR19-E03, and KM18-10**
106 **cruises (Nakamura, 2019; Nakamura, 2020a,b; JAMSTEC, 2004). Yellow dots indicate**
107 **epicenters of very low frequency earthquakes (Nakano et al. 2018; Takemura et al.**
108 **2019a,b; Takemura et al. 2022a,b) and green dots represent tremors (Ogiso and**
109 **Tamaribuchi 2022; Tamaribuchi et al. 2022). Blue and red stars indicate the epicenters of**
110 **the 1944 Tonankai and 1946 Nankai earthquakes, respectively. The rupture areas of these**
111 **earthquakes are represented by the red and blue dashed lines (Tanioka and Satake, 2001;**
112 **Baba et al., 2002). Black boxes indicate the location of Deep Sea Drilling Project/Ocean**
113 **Drilling Program/Integrated Ocean Drilling Program drill sites.**

114

115 ## 2 Data and Methods

116 Three dedicated seismic surveys were conducted between 2018 to 2020 (Nakamura,
117 2019; Nakamura, 2020a,b; JAMSTEC, 2004) that covered an area of approximately 250 km x
118 100 km from off Cape Shionomisaki to off Tosa Bay with line intervals between 4 to 8 km
119 (Figure 1). Large seismic sources (>120 L) were used and streamer cables 4-5.5 km long were
120 towed at a depth of 25 m to enhance reflections from deep features such as the top of the oceanic
121 basement. Reflection data was processed by Kirchhoff prestack depth migration (PreSDM).
122 Noise reduction and signal enhancement techniques included deghosting, designature,
123 debubbling, attenuation of surface-related multiples, and parabolic Radon transform filtering.
124 The dataset used in this study is the same dataset used by Nakamura et al. (2022) and the readers
125 are referred to their study for a detailed discussion on the data processing.
126 Key horizons tracked were the decollement and the top of oceanic crust. The decollement
127 was identified from the frontal thrust and its continuity was traced landward. The identification
128 was based on the common characteristics of detachment faults described by Shaw et al. (2005).
129 The top of the Philippine Sea Plate is the most easily identifiable horizon characterized by a
130 strong, positive, and high amplitude reflection. Taper angle was measured as the sum of the
131 seafloor slope (α) and decollement slope (β) 30 km from the frontal thrust. Decollement

roughness was measured by the root mean square (RMS) of its height from a reference line. The thickness of the underthrust sediments was calculated as the depth difference of the decollement and the top of oceanic crust. The effective friction of the decollement (μ_b) and the pore pressure ratio (λ^*) were calculated by applying the critical taper theory (Davis et al., 1983; Dahlen, 1984). The p-wave velocity model used for the PreSDM profiles were also used to estimate the λ^* of the underthrust sediments using the empirical relationships between p-wave velocity, porosity, and effective mean stress (Kitajima and Saffer, 2012). More details are provided in the supplementary file.

The study area was divided into four (4) zones based on the seismicity of slow earthquakes obtained by the previous studies (Figure 1). The geometrical and physical properties in each zone were then examined. Both VLFEs and tremors occur in the central part of the survey area where the subducted seamounts are also located. This area is defined as active zone 1 (AZ1) between lines 9 to 39. The easternmost part of the survey area between lines 49 to 56 is dominated by tremors with sporadic VLFEs is defined as AZ2. Gaps in slow earthquakes between lines 1 to 8 define quiet zone 1 (QZ1), while lines 40 to 48 define QZ2 (Figure 1,2). Previous studies have emphasized the large uncertainties in constraining the depth of slow earthquakes, thus we only focus on its along-strike distribution.

3 Seismic character of the decollement and underthrust

The decollement is generally traceable in the outer wedge and becomes untraceable in the inner wedge due to weak reflection, decollement step down, merging with the oceanic crust or duplex structures (Figure 3). Along-strike changes in the polarity of the decollement has been previously reported by Park et al. (2014) that may reflect changes in pore fluid pressures. Trench-parallel line SIE060 (Figure 3k) shows a strong, continuous, and negative polarity (blue) decollement. Trench-perpendicular lines SIN128, SIN140, SIN148, and KIN028 (Figure 3d-g) all show that the negative polarity decollement is traceable and becomes complex due to duplex structures. The negative polarity decollement observed in the survey lines from the KR19-E03 dataset agrees well with the observations of Park et al. (2014).

The decollement polarity for the KM20-05 and KM18-10 datasets could not be easily distinguished visually like the KR19-E03. However, the underthrust sediments clearly show along-strike changes in seismic signature. The underthrust is defined as the sediment package between the top of the oceanic basement and the floor thrust or the lowest level decollement. The floor thrust was favored over the roof thrust because we used the same horizon in calculating the taper angle. For example, survey line MS97-104 will have a different taper value when using the roof thrust (Figure 3c), which will also affect our μ_b and λ^* predictions. Additionally, the roof thrusts can be a different horizon and doesn't appear to be continuous with the decollement identified in the outer wedge such as lines SIN0822-1015, SIN1142-1011, and SIN128 (Figure 3a,b,d).

The underthrust sediments in the survey lines SIE060, SIN140, and SIN148 (Figure 3e,f,k) are generally transparent near the deformation front, while the other survey lines show a stratified underthrust. We interpret that the change in seismic signature may be due to a change in lithology as observed from drilling data. The decollement zone is located within the Lower Shikoku Basin (LSB) Facies. In Muroto, the LSB is composed entirely of hemipelagic

mudstones. On the other hand, the LSB in Ashizuri transect (off Tosa Bay) is comprised of sandy turbidites (Moore et al., 2001; Underwood 2007).

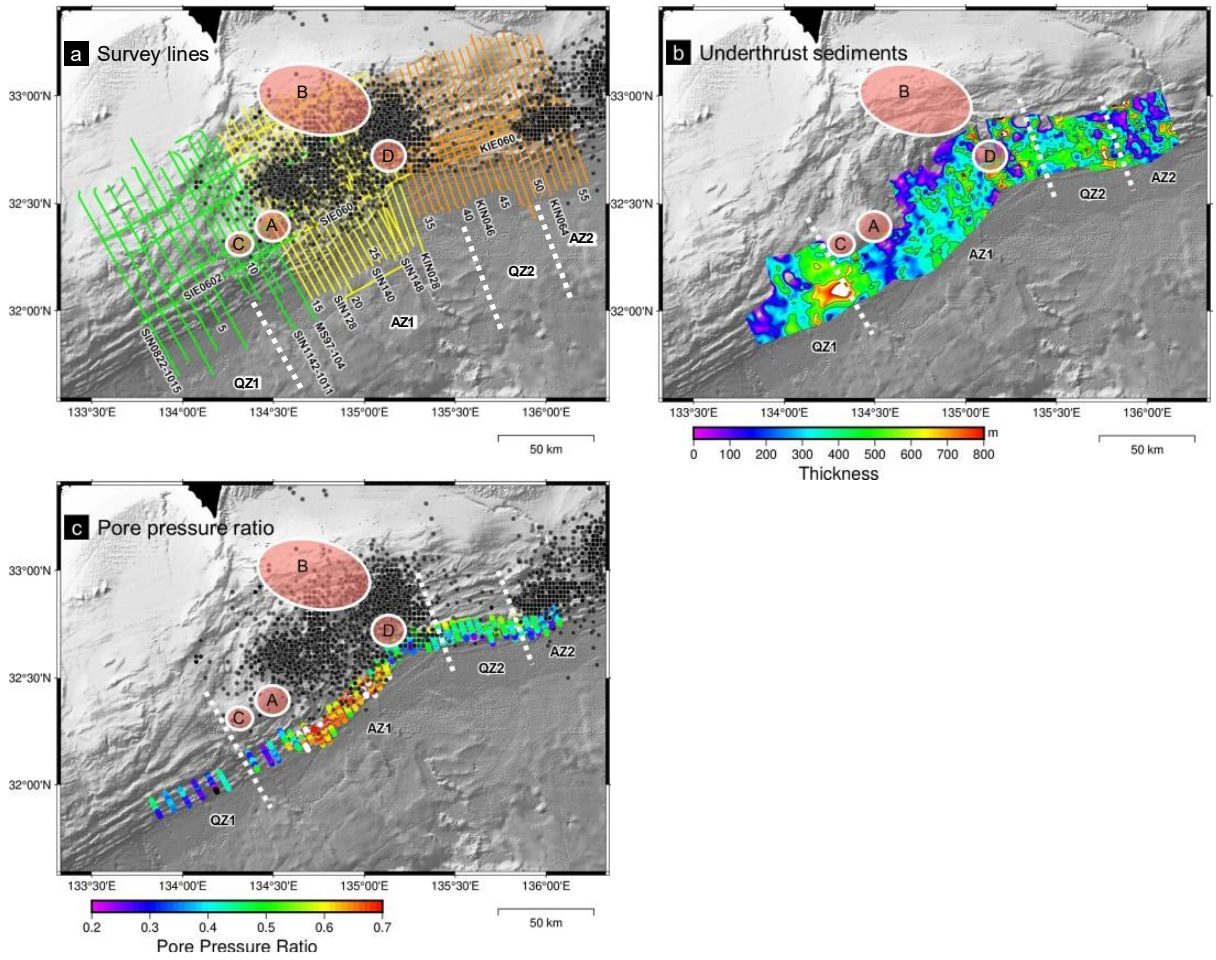

Figure 2. (a) A close-up view of the survey lines of the KM18-10 (orange), KR19-E03 (yellow), and KM20-05 (green) cruises from Figure 1. The active zones (AZ) and quiet zones (QZ) are marked by the white dashed line. (b) Thickness of underthrust sediments, which was calculated by the difference between the depths of the oceanic basement top and decollement. (c) Pore pressure ratio 10 km from the frontal thrust calculated from p-wave velocity. Black dots indicate the epicenters of slow earthquakes. Red circles with white outline are subducted seamounts proposed by Park et al. (1999) – A, Kodaira et al. (2000) – B, and Nakamura et al. (2022) – C, D. Areas with high activity of slow earthquakes are labelled as active zones (AZ) while areas with no slow earthquakes are quiet zones (QZ).

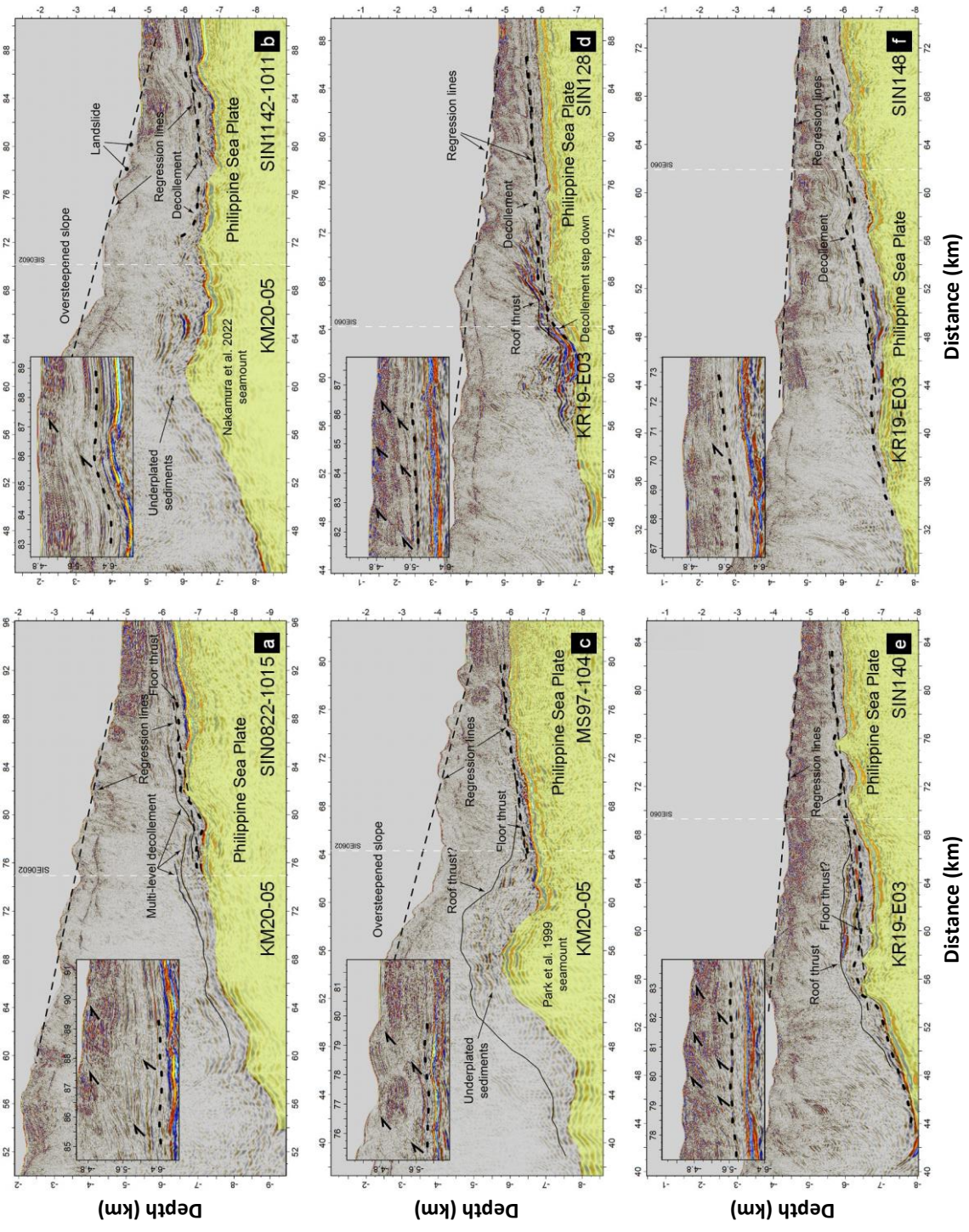
a
SIN0822-1015
KM20-05
Philippine Sea Plate
Multi-level decollement
Regression lines
Floor thrust
b
SIN1142-1011
KM20-05
Philippine Sea Plate
Landside
Regression lines
Decollement
Oversteepened slope
Underplated sediments
Nakamura et al. 2022 seamount
c
MS97-104
KM20-05
Philippine Sea Plate
Oversteepened slope
Roof thrust?
Regression lines
Floor thrust
Underplated sediments
Park et al. 1999 seamount
d
SIN128
KR19-E03
Philippine Sea Plate
Regression lines
Decollement
Roof thrust
Decollement step down
e
SIN140
KR19-E03
Philippine Sea Plate
Regression lines
Roof thrust
Floor thrust?
f
SIN148
KR19-E03
Philippine Sea Plate
Regression lines
Decollement
Depth (km)
Distance (km)

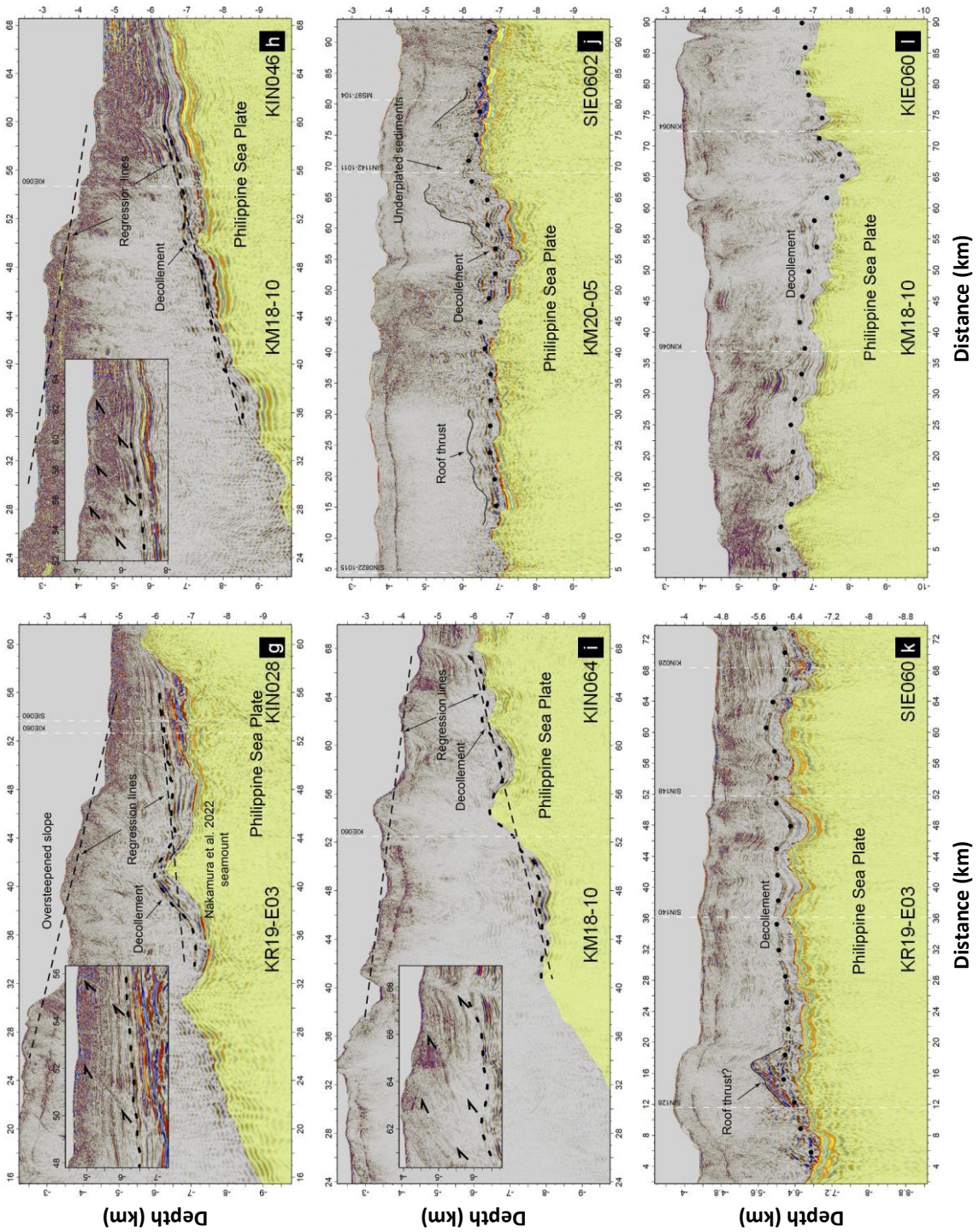

Figure 3. Interpretation of representative seismic profiles. The location of the survey lines are indicated in Figure 2a. The decollement or floor thrusts are thick black dashed lines, while roof thrusts are thin solid black lines. The linear fit or regression line of the seafloor and the decollement are thin dashed lines. The slope of the regression lines were used to calculate the taper angle. The subplot in each figure is a close-up view of the frontal thrust area. Uninterpreted versions are provided in the supplementary file.

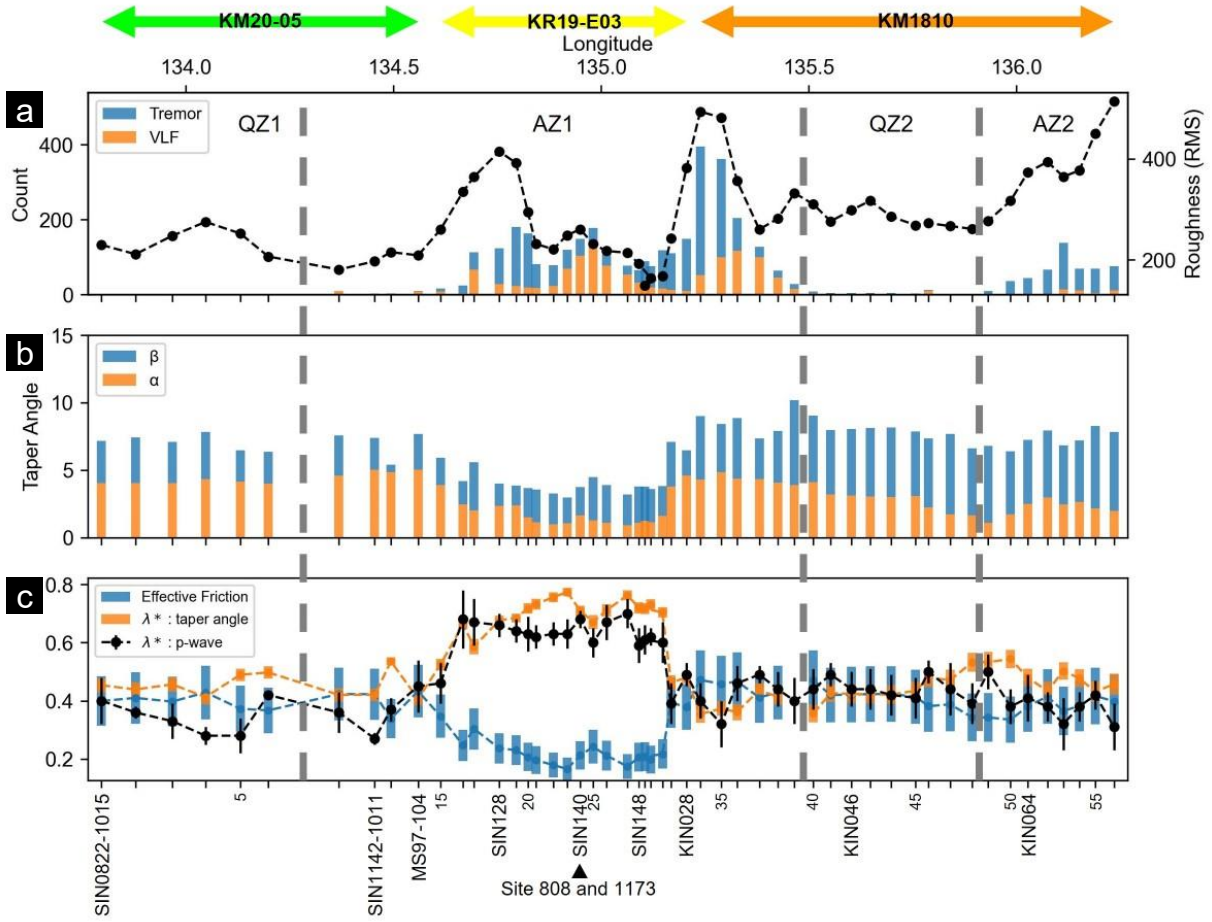

Figure 4. (a) The number of tremor and very low frequency earthquakes superimposed with the roughness of the decollement (black line). (b) The apparent seafloor slope (α) and basal slope (β) calculated from the seismic profiles. (c) The estimated effective basal friction (μ_b) and pore pressure ratio (λ^*) calculated from the taper angle and p-wave velocity. The quiet (QZ) and active zones (AZ) are marked by the gray dashed vertical lines.

4 Association of slow earthquake activity with decollement roughness and underthrust thickness

The streamer cable used was 6 km, hence, there are limitations to the accuracy of the velocity models to create the PreSDM profiles especially in the deeper portions where it is expected to be less accurate. To overcome this challenge, we only used the shallowest part of our dataset and only limited our analysis to where we can confidently trace the decollement (Figure 2b). The number of VLFEs (Nakano et al. 2018; Takemura et al. 2019a,b; Takemura et al. 2022a,b) and tremors (Ogiso and Tamaribuchi 2022; Tamaribuchi et al. 2022) within a 2.15 km rectangular buffer from each survey line was compared with the decollement roughness. The buffer size was based on the average spacing between all the survey lines. The average decollement roughness is highest at AZ2 (368±104m) and it is relatively the same in QZ1

(240±82 m), QZ2 (295±74 m), and AZ1 (271±147 m). However, the standard deviation of the RMS, which is representative of the along-strike roughness of each zone is higher in the active zones because of the presence of multiple subducted seamounts or bathymetric highs.

Another key feature within AZ1 is the smooth decollement (low RMS) between lines 21 to 31 (206±57 m) (Figure 4). Comparison with the trench-perpendicular profiles in the KR19-E03 area such as lines SIN128, SIN140, and SIN148 (Figure 2,3d-f) shows that the underthrust sediments have a relatively uniform thickness at the deformation front but becomes thinner landward because of step down or merging with the oceanic basement top. In this case, if we treat the oceanic basement top to be the same as the decollement or plate boundary fault, the association between a rough decollement and slow earthquake activity still holds true.

5 Taper angle variations

Comparison between the apparent and true taper angle were only conducted on selected profiles in the KM18-10 and KR19-E03 survey area because the survey lines from the KM20-05 research cruise is generally perpendicular to the trench axis (Supplementary). The root mean square error (RMSE) between the apparent and true α and β due to the azimuth difference is only 0.1°, hence the apparent taper angle is considered representative of the along-strike changes in taper values (Figure 4). A significant decrease in taper angle is observed within AZ1 between survey lines 17 to 31 (α_{ave} = 1.4°, β_{ave} = 2.4°) that coincides with the dent in the trench likely due to the subduction of the seamounts (Figure 4). The low taper angle in Muroto has already been recognized from previous studies (Kimura et al., 2007; Park et al. 2014) but in this study we were able to map the lateral extent of the decreased taper from the dense seismic reflection data. The rapid change in taper values from lines 27 (3.2°) to 34 (9.0°) is also considered a true feature because survey line SIN148 and line 30 which intersect near the frontal thrust have almost the same taper values despite having different azimuth (Figure 2,4).

The change in taper angle between Muroto and Ashizuri (off Tosa Bay) was attributed by Saffer (2010) to the lithology of the LSB facies. Numerical simulations showed that the turbidite-rich LSB facies in Ashizuri is up to 100 times more permeable compared to LSB facies in Muroto which is comprised entirely of mudstone (Moore et al., 2001; Underwood, 2007; Saffer, 2010). The high permeability of turbidite-rich sediments allows for better drainage of fluids, resulting in lower pore pressures and higher taper angle values. A similar mechanism can also be in effect between Muroto and Kumano based on the seismic character of the underthrust discussed in section 3.

6 Comparison of effective friction and pore pressure ratio estimates with previous studies

The calculated effective friction (μ_b) and pore pressure ratio based on the critical taper theory ($\lambda^*_{\alpha+\beta}$) was assessed by comparing the μ_b and $\lambda^*_{\alpha+\beta}$ obtained from the apparent and true taper values 30 km from the frontal thrust, and comparison with published results. We found negligible difference of the μ_b and the $\lambda^*_{\alpha+\beta}$ calculated from the apparent and true taper angle with an RMSE of only 0.01 (Supplementary). Survey line SIN140 is close to drill sites 808 and 1173 where μ_b and the $\lambda^*_{\alpha+\beta}$ were determined by previous studies from laboratory experiments. In site 808, Kopf and Brown (2003) reported that μ_b ranges from 0.16 to 0.26, and λ^* can be up to 0.85. In site 1173, Brown et al. (2003) determined that μ_b is around 0.32, and λ^* ranges from 0.6 to 0.8. Tsuji et al. (2008) also estimated that λ^* in Muroto ranges from 0.4 to 0.7 based on

seismic velocity data. Our results for SIN140 show that μ_b ranges from 0.16 to 0.26, and λ^* ranges from 0.69 to 0.73 (Figure 4), which coincides well with the values reported from previous studies.

The calculated pore pressure ratio from p-wave velocity (λ^*_{Vp}) was compared with the results of Tsuji et al. (2008, Fig 4) and Tobin and Saffer (2009, Fig 2). The vertical profile of the calculated pore pressure, hydrostatic pressure, and vertical confining stress from the velocity model of line SIN140 near the drill site 808 show a good fit with the results of Tsuji et al. (2008) for the same parameters (Supplementary). This indicates that our velocity model near the frontal thrust is consistent with previous studies. The accuracy of velocities determined from seismic data decreases landward (Tsuji et al., 2008), hence it is important to determine the distance from the trench at which our velocity model is considered accurate. High pore pressure decreases the effective normal stress and promotes the occurrence of slow earthquakes (Kitajima and Saffer, 2012). The effective stress in the underthrust sediments of line SIN140 is relatively constant ~10 MPa from the trench up to 10 km landward, then increases to ~25 MPa 20 km landward (Supplementary). However, results of Tobin and Saffer (2009) indicate that the effective stress at the trench is ~5 MPa and slowly increases to ~9 MPa 20 km landward. Thus, we only considered the 10 km distance from the frontal thrust calculate the λ^*_{Vp} because of the consistent trend in our results and the results of Tobin and Saffer (2009) where the effective stress is relatively constant over this distance.

The $\lambda^*_{\alpha+\beta}$ and λ^*_{Vp} show high correlation (0.8) and both dataset shows elevated pore pressures off Muroto (Figure 4). The decrease in taper angle within AZ1 from survey lines 17 to 31 translates to a wide zone of low μ_b and high λ^* that coincides with the high slow earthquake activity off Muroto. It is important to note that $\lambda^*_{\alpha+\beta}$ and λ^*_{Vp} were calculated 30 km and 10 km from the frontal thrust, respectively, and the downdip extent of slow earthquake activity extends further landward (Figure 1,2). We assume that our calculated pore pressure conditions may extend deeper or at least exhibit the same trend where Muroto has elevated λ^* than surrounding areas mainly because of the consistent results between $\lambda^*_{\alpha+\beta}$ and λ^*_{Vp}. Hirose et al. (2021) reported the first direct evidence of high pore pressure in Muroto and their numerical model suggests a patch-like distribution of high pore pressure zones. Our results possibly indicate that these high pore pressure patches can be found over a wide area.

The calculated high λ^* zone in this study does not extend further eastward to cover the area between lines 32 to 39 in AZ1. Additionally, AZ2 also exhibits similar λ^* with the quiet zones (Figure 4). Assuming that the high λ^* at the frontal wedge extends landward, this possibly indicates that slow earthquakes do not always occur in areas with high λ^* but in combination other variables such as decollement roughness. Our results further shows that slow earthquake gaps may be related to both low λ^* and a smooth decollement (Figure 4). A possible factor that can explain the decreased λ^* in lines 32 to 39 is a change in lithology of the underthrust sediments. Survey line SIN148 has a transparent underthrust while lines KIN028 and KIN046 have a stratified underthrust (Figure 3f-h). This possible change in lithology affects pore fluid pressures and taper angle as discussed in sections 3 and 5.

7 Proposed mechanism for the high pore pressure in Muroto

The high λ^* in Muroto is likely due to seamount subduction and sediment underplating. The presence of underplated sediments has already been noted by previous studies (Leggett et al., 1985; Park et al., 1999; Park et al., 2002). The underplated sediments are best observed in

survey lines within AZ1 such as SIN1142-1011, MS97-104, SIN128, and SIN140 (Figure 3b-e), which is characterized as a reflective unit located in the deep strong reflector zone defined by Park et al. (2002). The formation of the underplated sediments has been typically associated with duplexing (Leggett et al., 1985; Park et al., 1999; Park et al., 2002). However, we propose an alternative mechanism for sediment underplating, which follows the results of Dominguez et al. (2000) from sandbox models.

One of the key findings of Dominguez et al. (2000) is that the seamount drags down a large volume of trench-fill sediments while it is being subducted and will eventually leave it behind as subduction continues. This sediment package is the underplated sediments and its volume can be 2-3 times larger than the volume of the seamount (Dominguez et al., 2000). A recent study by Bangs et al. (2023) in the Hikurangi margin reported a sediment lens trailing a subducting seamount can be a possible real-world example of the sediment underplating observed by Dominguez et al. (2000). In the Makran subduction zone, numerical simulations by Pajang et al. (2022) on the effect of seamount subduction produced a large thrust slice after a seamount is subducted, which is also consistent with the underplated structure seen in this study (Figure 3). This implies that the subduction of the 13 km thick and 50 km wide seamount identified by Kodaira et al. (2000) could have led to widespread underplating of fluid-rich trench-fill sediments. Due to compression from the newly subducted seamounts identified by Park et al. (1999) and Nakamura et al. (2022), the fluids in the underplated sediments may have been expelled and redistributed along the decollement. A new batch of underplated sediments may have also been introduced by the newly subducted seamounts. This mechanism best explains the observations of Moore et al. (2001) where they reported similar chemical characteristics of fluids between the trench fill sediments at site 1174, a potential deep fluid source at site 1176 that may be associated with the splay fault (Figure 1), and the fluid in the low-Cl zone centered below the decollement. Our proposed mechanism of fluid expulsion from the underplated sediments, and the effect of lithology of the LSB facies (Saffer, 2010) potentially explains the wide zone of high λ^* in Muroto.

8 Conclusions

We showed the spatial association or correspondence of slow earthquake activity with along strike geometrical changes in the Nankai Trough such as decollement roughness and prism taper angle, and physical property changes such as μ_b and λ^*. The geometrical and physical properties described in this study are located in the updip region of where slow earthquakes occur. However, we still observed a correspondence that may explain the spatial distribution of slow earthquakes. We assume that the calculated λ^* may extend deeper or at least exhibit a similar trend where Muroto has elevated λ^* because of the good agreement between $\lambda^*_{\alpha+\beta}$ and λ^*_{Vp} calculated 30 km and 10 km from the frontal thrust, respectively. We also highlight the possible role of multiple seamount subduction for slow earthquake activity off Muroto. The major findings can be summarized below:

1. Slow earthquake activity is not simply associated with high λ^* but in combination with other variables. Slow earthquake gaps were observed in areas with both low λ^* and a smooth decollement.
2. The spatial extent of the low taper angle in Muroto was mapped and it coincides with the dent in the Nankai Trough and the region of high slow earthquake activity. The low taper angle in Muroto translates to a wide zone of low μ_b and high λ^* composed of patches of overpressured aquifers (Hirose et al., 2021).

3. We propose that the fluid source off Muroto is due to fluid expulsion from underplated fluid-rich trench-fill sediments. Underplating was caused by the subduction of the seamount identified by Kodaira et al. (2000), and fluid expulsion was caused by the compression from the newly subducted seamounts identified by Park et al. (1999) and Nakamura et al. (2022). This mechanism combined with hydrologic effects due to the change in lithology of the LSB facies (Saffer, 2010) likely caused the high λ^* off Muroto.

Acknowledgments

The authors are grateful to the anonymous reviewers for their valuable comments and suggestions. Partial funding was also provided by the Yokohama National University through Project C of Kankyo-Joho.

Open Research

Seismic data used in this study are available at the JAMSTEC seismic survey database https://www.jamstec.go.jp/obsmcs_db/e/index.html. Specify the year (2018, 2019, 2020) and cruise (KM18-10, KR19-E03, KM20-05) and proceed to the page of data request https://www.jamstec.go.jp/obsmcs_db/form/obsmcs_db_entry_e/.

Bibliography

Araki, E., Saffer, D. M., Kopf, A. J., Wallace, L. M., Kimura, T., Machida, Y., . . . Rösner, A. (2017, June). Recurring and triggered slow-slip events near the trench at the Nankai Trough subduction megathrust. *Science, 356*, 1157–1160. doi:10.1126/science.aan3120

Baba, S., Araki, E., Yamamoto, Y., Hori, T., Fujie, G., Nakamura, Y., . . . Matsumoto, H. (2023, June). Observation of Shallow Slow Earthquakes by Distributed Acoustic Sensing Using Offshore Fiber-Optic Cable in the Nankai Trough, Southwest Japan. *Geophysical Research Letters, 50*. doi:10.1029/2022gl102678

Bangs, N. L., Morgan, J. K., Bell, R. E., Han, S., Arai, R., Kodaira, S., . . . Fry, B. (2023, June). Slow slip along the Hikurangi margin linked to fluid-rich sediments trailing subducting seamounts. *Nature Geoscience, 16*, 505–512. doi:10.1038/s41561-023-01186-3

Brown, K. M., Kopf, A., Underwood, M. B., & Weinberger, J. L. (2003, September). Compositional and fluid pressure controls on the state of stress on the Nankai subduction thrust: A weak plate boundary. *Earth and Planetary Science Letters, 214*, 589–603. doi:10.1016/s0012-821x(03)00388-1

Chesley, C., Naif, S., Key, K., & Bassett, D. (2021, July). Fluid-rich subducting topography generates anomalous forearc porosity. *Nature, 595*, 255–260. doi:10.1038/s41586-021-03619-8

Dahlen, F. A. (1984, November). Noncohesive critical Coulomb wedges: An exact solution. *Journal of Geophysical Research: Solid Earth, 89*, 10125–10133. doi:10.1029/jb089ib12p10125

Dahlen, F. A., Suppe, J., & Davis, D. (1984, November). Mechanics of fold-and-thrust belts and accretionary wedges: Cohesive Coulomb Theory. *Journal of Geophysical Research: Solid Earth, 89*, 10087–10101. doi:10.1029/jb089ib12p10087

Davis, D., Suppe, J., & Dahlen, F. A. (1983). Mechanics of fold-and-thrust belts and accretionary wedges. *Journal of Geophysical Research, 88*, 1153. doi:10.1029/jb088ib02p01153

Dominguez, S., Malavieille, J., & Lallemand, S. E. (2000, February). Deformation of accretionary wedges in response to seamount subduction: Insights from sandbox experiments. *Tectonics, 19*, 182–196. doi:10.1029/1999tc900055

Ellis, S., Fagereng, Å., Barker, D., Henrys, S., Saffer, D., Wallace, L., . . . Harris, R. (2015, April). Fluid budgets along the northern Hikurangi subduction margin, New Zealand: the effect of a subducting seamount on fluid pressure. *Geophysical Journal International, 202*, 277–297. doi:10.1093/gji/ggv127

Hirose, T., Hamada, Y., Tanikawa, W., Kamiya, N., Yamamoto, Y., Tsuji, T., . . . Kubo, Y. (2021, June). High Fluid-Pressure Patches Beneath the Décollement: A Potential Source of Slow Earthquakes in the Nankai Trough off Cape Muroto. *Journal of Geophysical Research: Solid Earth, 126*. doi:10.1029/2021jb021831

Ide, S., & Beroza, G. C. (2023, July). Slow earthquake scaling reconsidered as a boundary between distinct modes of rupture propagation. *Proceedings of the National Academy of Sciences, 120*. doi:10.1073/pnas.2222102120

Ide, S., Beroza, G. C., Shelly, D. R., & Uchide, T. (2007, May). A scaling law for slow earthquakes. *Nature, 447*, 76–79. doi:10.1038/nature05780

Ike, T., Moore, G. F., Kuramoto, S., Park, J.-O., Kaneda, Y., & Taira, A. (2008, September). Variations in sediment thickness and type along the northern Philippine Sea Plate at the Nankai Trough. *Island Arc, 17*, 342–357. doi:10.1111/j.1440-1738.2008.00624.x

JAMSTEC. (2004). JAMSTEC Seismic Survey Database. *JAMSTEC Seismic Survey Database* [Dataset]. JAMSTEC. https://doi.org/10.17596/0002069

Kato, A., Obara, K., Igarashi, T., Tsuruoka, H., Nakagawa, S., & Hirata, N. (2012, February). Propagation of Slow Slip Leading Up to the 2011\less{}{i}{}\greater{}{M}{}\less{}{/}{i}\greater{}{}{\less{}{s}{u}}b\greater{}{w}{}\less{}{/}{s}ub\greater{}{9}{.}0 Tohoku-Oki Earthquake. *Science, 335*, 705–708. doi:10.1126/science.1215141

Kimura, G., Kitamura, Y., Hashimoto, Y., Yamaguchi, A., Shibata, T., Ujiie, K., & Okamoto, S. (2007, March). Transition of accretionary wedge structures around the up-dip limit of the seismogenic subduction zone. *Earth and Planetary Science Letters, 255*, 471–484. doi:10.1016/j.epsl.2007.01.005

Kitajima, H., & Saffer, D. M. (2012, December). Elevated pore pressure and anomalously low stress in regions of low frequency earthquakes along the Nankai Trough subduction megathrust. *Geophysical Research Letters, 39*, n/a–n/a. doi:10.1029/2012gl053793

Kodaira, S., Iidaka, T., Kato, A., Park, J.-O., Iwasaki, T., & Kaneda, Y. (2004, May). High Pore Fluid Pressure May Cause Silent Slip in the Nankai Trough. *Science, 304*, 1295–1298. doi:10.1126/science.1096535

Kodaira, S., Takahashi, N., Nakanishi, A., Miura, S., & Kaneda, Y. (2000, July). Subducted Seamount Imaged in the Rupture Zone of the 1946 Nankaido Earthquake. *Science, 289*, 104–106. doi:10.1126/science.289.5476.104

Kopf, A., & Brown, K. M. (2003, November). Friction experiments on saturated sediments and their implications for the stress state of the Nankai and Barbados subduction thrusts. *Marine Geology, 202*, 193–210. doi:10.1016/s0025-3227(03)00286-x

Leeman, J. R., Saffer, D. M., Scuderi, M. M., & Marone, C. (2016, March). Laboratory observations of slow earthquakes and the spectrum of tectonic fault slip modes. *Nature Communications, 7*. doi:10.1038/ncomms11104

Leggett, J., Aoki, Y., & Toba, T. (1985, May). Transition from frontal accretion to underplating in a part of the Nankai Trough Accretionary Complex off Shikoku (SW Japan) and extensional features on the lower trench slope. *Marine and Petroleum Geology, 2*, 131–141. doi:10.1016/0264-8172(85)90003-0

Liu, Y., & Rice, J. R. (2007, September). Spontaneous and triggered aseismic deformation transients in a subduction fault model. *Journal of Geophysical Research: Solid Earth, 112*. doi:10.1029/2007jb004930

Moore, G. F., Taira, A., Klaus, A., Becker, L., Boeckel, B., Cragg, B. A., . . . Wilson, M. (2001, October). New insights into deformation and fluid flow processes in the Nankai Trough accretionary prism: Results of Ocean Drilling Program Leg 190. *Geochemistry, Geophysics, Geosystems, 2*, n/a–n/a. doi:10.1029/2001gc000166

Nakamura, Y. (2019). R/V Kaimei Cruise Report KM18-10. *R/V Kaimei Cruise Report KM18-10* [Dataset]. JAMSTEC. https://doi.org/10.17596/0002663

Nakamura, Y. (2020). R/V Kaimei "Cruise Report" KM20-05. *R/V Kaimei "Cruise Report" KM20-05* [Dataset]. JAMSTEC. https://doi.org/10.17596/0002555

Nakamura, Y. (2020). R/V Kairei Cruise Report KR19-E03_leg1-2. *R/V Kairei Cruise Report KR19-E03_leg1-2* [Dataset]. JAMSTEC. https://doi.org/10.17596/0002618

Nakamura, Y., Shiraishi, K., Fujie, G., Kodaira, S., Kimura, G., Kaiho, Y., . . . Miura, S. (2022, May). Structural Anomaly at the Boundary Between Strong and Weak Plate Coupling in the Central-Western Nankai Trough. *Geophysical Research Letters, 49*. doi:10.1029/2022gl098180

Nakano, M., Hori, T., Araki, E., Kodaira, S., & Ide, S. (2018, March). Shallow very-low-frequency earthquakes accompany slow slip events in the Nankai subduction zone. *Nature Communications, 9*. doi:10.1038/s41467-018-03431-5

Nishikawa, T., Ide, S., & Nishimura, T. (2023, January). A review on slow earthquakes in the Japan Trench. *Progress in Earth and Planetary Science, 10*. doi:10.1186/s40645-022-00528-w

Ogiso, M., & Tamaribuchi, K. (2022, March). Spatiotemporal evolution of tremor activity near the Nankai Trough trench axis inferred from the spatial distribution of seismic amplitudes. *Earth, Planets and Space, 74*. doi:10.1186/s40623-022-01601-w

Okamoto, A. S., Niemeijer, A. R., Takeshita, T., Verberne, B. A., & Spiers, C. J. (2020, March). Frictional properties of actinolite-chlorite gouge at hydrothermal conditions. *Tectonophysics, 779*, 228377. doi:10.1016/j.tecto.2020.228377

Pajang, S., Khatib, M. M., Heyhat, M., Cubas, N., Bessiere, E., Letouzey, J., . . . Le Pourhiet, L. (2022, December). The distinct morphologic signature of underplating and seamounts in accretionary prisms, insights from thermomechanical modeling applied to Coastal Iranian Makran. *Tectonophysics, 845*, 229617. doi:10.1016/j.tecto.2022.229617

Park, J.-O., & Hondori, E. J. (2023, July). Link between the Nankai underthrust turbidites and shallow slow earthquakes. *Scientific Reports, 13*. doi:10.1038/s41598-023-37474-6

Park, J.-O., Naruse, H., & Bangs, N. L. (2014, October). Along-strike variations in the Nankai shallow décollement properties and their implications for tsunami earthquake generation. *Geophysical Research Letters, 41*, 7057–7064. doi:10.1002/2014gl061096

Park, J.-O., Tsuru, T., Kaneda, Y., Kono, Y., Kodaira, S., Takahashi, N., & Kinoshita, H. (1999, April). A subducting seamount beneath the Nankai Accretionary Prism off Shikoku, southwestern Japan. *Geophysical Research Letters, 26*, 931–934. doi:10.1029/1999gl900134

Park, J.-O., Tsuru, T., Takahashi, N., Hori, T., Kodaira, S., Nakanishi, A., . . . Kaneda, Y. (2002, April). A deep strong reflector in the Nankai accretionary wedge from multichannel seismic data: Implications for underplating and interseismic shear stress release. *Journal of Geophysical Research: Solid Earth, 107*, ESE 3–1–ESE 3–16. doi:10.1029/2001jb000262

Saffer, D. M. (2010, March). Hydrostratigraphy as a control on subduction zone mechanics through its effects on drainage: an example from the Nankai Margin, SW Japan. *Geofluids*. doi:10.1111/j.1468-8123.2009.00276.x

Sun, T., Saffer, D., & Ellis, S. (2020, March). Mechanical and hydrological effects of seamount subduction on megathrust stress and slip. *Nature Geoscience, 13*, 249–255. doi:10.1038/s41561-020-0542-0

Takemura, S., Baba, S., Yabe, S., Emoto, K., Shiomi, K., & Matsuzawa, T. (2022, May). Source Characteristics and Along-Strike Variations of Shallow Very Low Frequency Earthquake Swarms on the Nankai Trough Shallow Plate Boundary. *Geophysical Research Letters, 49*. doi:10.1029/2022gl097979

Takemura, S., Matsuzawa, T., Noda, A., Tonegawa, T., Asano, Y., Kimura, T., & Shiomi, K. (2019, April). Structural Characteristics of the Nankai Trough Shallow Plate Boundary Inferred From Shallow Very Low Frequency Earthquakes. *Geophysical Research Letters, 46*, 4192–4201. doi:10.1029/2019gl082448

Takemura, S., Noda, A., Kubota, T., Asano, Y., Matsuzawa, T., & Shiomi, K. (2019, November). Migrations and Clusters of Shallow Very Low Frequency Earthquakes in the Regions Surrounding Shear Stress Accumulation Peaks Along the Nankai Trough. *Geophysical Research Letters, 46*, 11830–11840. doi:10.1029/2019gl084666

Takemura, S., Obara, K., Shiomi, K., & Baba, S. (2022, February). Spatiotemporal Variations of Shallow Very Low Frequency Earthquake Activity Southeast Off the Kii Peninsula, Along the Nankai Trough, Japan. *Journal of Geophysical Research: Solid Earth, 127*. doi:10.1029/2021jb023073

Tamaribuchi, K., Ogiso, M., & Noda, A. (2022, August). Spatiotemporal Distribution of Shallow Tremors Along the Nankai Trough, Southwest Japan, as Determined From Waveform

Amplitudes and Cross-Correlations. *Journal of Geophysical Research: Solid Earth, 127*. doi:10.1029/2022jb024403

Tilley, H., Moore, G. F., Underwood, M. B., Hernández-Molina, F. J., Yamashita, M., Kodaira, S., & Nakanishi, A. (2021, October). Heterogeneous Sediment Input at the Nankai Trough Subduction Zone: Implications for Shallow Slow Earthquake Localization. *Geochemistry, Geophysics, Geosystems, 22*. doi:10.1029/2021gc009965

Tobin, H. J., & Saffer, D. M. (2009, July). Elevated fluid pressure and extreme mechanical weakness of a plate boundary thrust, Nankai Trough subduction zone. *Geology, 37*, 679–682. doi:10.1130/g25752a.1

Tsuji, T., Tokuyama, H., Pisani, P. C., & Moore, G. (2008, November). Effective stress and pore pressure in the Nankai accretionary prism off the Muroto Peninsula, southwestern Japan. *Journal of Geophysical Research, 113*. doi:10.1029/2007jb005002

Underwood, M. B. (2007, December). 3. Sediment Inputs to Subduction Zones. In *The Seismogenic Zone of Subduction Thrust Faults* (pp. 42–85). Columbia University Press. doi:10.7312/dixo13866-003

Wang, K., & Bilek, S. L. (2011, August). Do subducting seamounts generate or stop large earthquakes? *Geology, 39*, 819–822. doi:10.1130/g31856.1

Yokota, Y., Ishikawa, T., Watanabe, S.-i., Tashiro, T., & Asada, A. (2016, May). Seafloor geodetic constraints on interplate coupling of the Nankai Trough megathrust zone. *Nature, 534*, 374–377. doi:10.1038/nature17632